IAF-95-U.4.08
DESIGN AND QUALIFICATION OF THE EXTREME-UV IMAGING TELESCOPE

J.M. Defise*, P. Rochus†
Centre Spatial de Liège , University of Liège, Belgium

Abstract.

A global optical survey of the solar corona will be accomplished by observations made with an **Extreme ultraviolet Imaging Telescope** (**EIT**), an experiment on-board of SOHO. EIT is a high resolution, wide field, multi-bandpass, Ritchey-Chretien telescope providing in the focal plane, images of the solar disk at four wavelengths in the EUV range (He II-30.4 nm-6 10^4 K ; Fe IX-17.1 nm-10^6 K ; Fe XII-19.5 nm-1.6 10^6 K; Fe XV-28.4 nm-3 10^6 K). The images in four narrow bandpasses will be obtained using 4 normal incidence multilayered coatings, deposited on quadrants of the mirrors. They will be recorded on a specific CCD camera especially developed for EIT. The concept design, the main key technologies used in the instrument and its main specificities are presented as well as the development, the integration, the tests and qualification philosophy. We emphasise the critical points of the design: the compactness (4 telescopes in one), the image quality, the thermal control, the alignment, the pointing stability and the dynamical constraints. Some lessons learned for future design are outlined.

1. Introduction.

1.1 EIT and the SOHO mission.

The EIT (Extreme UV Imaging Telescope) is an instrument developed in the frame of a collaboration between IAS at Orsay (F), IOTA at Orsay (F), LAS at Marseille (F), NRL at Washington (USA), LPARL at Palo Alto (USA) and Centre Spatial de Liège (B).

The Solar Heliospheric Observatory (SOHO spacecraft) is part of the international STSP program of ESA and NASA. Launched end 1995, SOHO will reach the Ll Lagrangian point located between Earth and the Sun, at 1,500,000 km from Earth. It will stay on a "halo orbit" around this location (figure (1)).

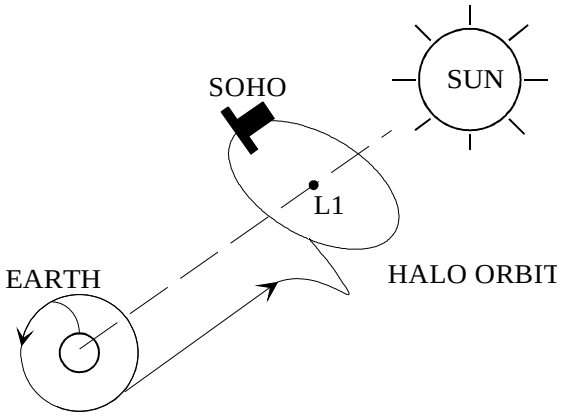

Figure (1): The halo orbit around L1.

SOHO (figure (2)) will become a fixed observatory oriented towards the sun. It is a 3 axes stabilised sun pointing spacecraft within 10 arcsec stability over 6 months (1 arcsec stability over 1.5 min) that will provide 2 to 6 years of continuous observations without any eclipse for all the on-board experiments.

* Project engineer, Centre Spatial de Liège (Belgium)
† Director of R & D department, Centre Spatial de Liège (Belgium)

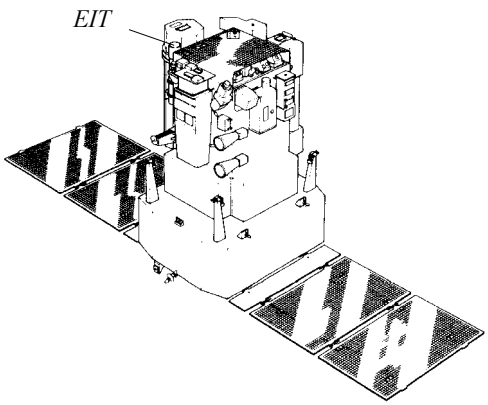

Figure (2): The SOHO spacecraft.

The solar corona and the solar wind will be monitored and analysed from the L1 point by a new package of 12 instruments. The SOHO mission will provide an opportunity for substantial data from solar and heliospheric observations. It is planned for a nominal duration of two years with an optional extension to six year.

The main objectives of the SOHO mission are

- the study and the understanding of the solar coronal phenomena and the solar wind.
- the study of the solar structure and the interior dynamics from its core to the photosphere.

Among these solar experiments attached to a 2000 kg spacecraft, EIT is a medium imaging telescope of the 15 kg class. The EIT experiment is a multi-bandpass Ritchey-Chretien telescope providing in the focal plane images of the solar disk at four wavelengths in the EUV range (He II-30.4 nm-6 10^4 K ; Fe IX-17.1 nm-10^6 K ; Fe XII-19.5 nm-1.6 10^6 K; Fe XV-28.4 nm-3 10^6 K). The experiment is a high resolution, wide field telescope that will produce images of the corona on the disk and above the solar limb.

With its capacity to distribute in real time data to the other coronal instruments on SOHO, EIT will play the role of "conductor" among the instruments on SOHO, dedicated to the corona and chromosphere. With its good corona coverage, EIT will inform the other instruments about the interesting zones to be analysed.

2. The EIT instrument.

2.1 The optical layout.

Sun images will be taken successively in 4 narrow bandpasses of the extreme ultraviolet range defined by multilayered coatings deposited on normal incidence optics. These mirrors form a Ritchey-Chretien telescope with a wide field of view and high spatial resolution. A rotating mask, occulting three quarters of the primary mirror, is used to select a given quadrant, corresponding to a given bandpass, as sketched in figure (3).

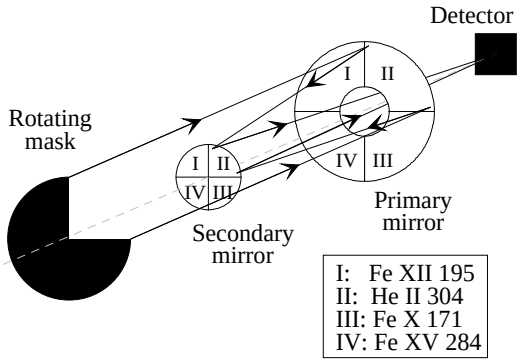

Figure (3): The EIT optical layout, including 4 telescopes in one.

This concept of 4 telescopes in one provides savings of essential resources, as mass and volume. It also ensures with a single detector, an accurate and stable co-alignment of the 4 types of images.

The optical system, with a focal length of 1650 mm, provides a spatial resolution of 1 arcsec on the scientific field of view, which is a great advantage compared to grazing incidence telescope having off-axis image degradation.

The normal incidence and the high filtering in narrow bandpasses is obtained by interferometric effects in multilayered coatings realised on the two mirrors. The EUV bandpasses of the four observing channels are designed to isolate different temperature plasmas in each channel. The combination of the aluminium filters and the multilayers on the mirrors will provide quasi-isothermal images of the sun.

The images are collected by a CCD camera (refer to figure (4)). The detector, with 1024 x 1024 pixels, is a SITE/TEKTRONIX specific back thinned CCD, for an efficient UV sensitivity. The 21 µm pixel size leads to an effective resolution of 2.6 arcsec.

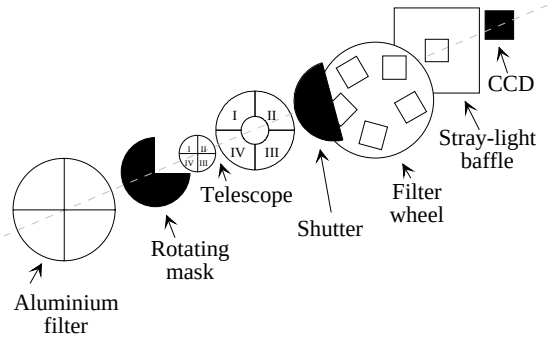

Figure (4): Schematics of EIT.

After rejection of the visible light with a specific aluminium filter, the remaining EUV flux is collected by the optics, then is imaged on the CCD detector.

2.2 The mechanical layout.

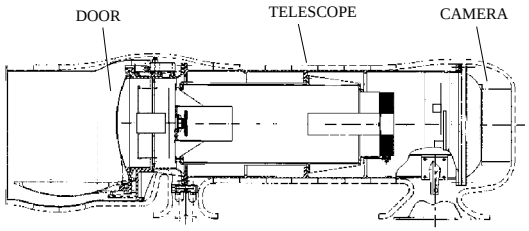

Figure (5): The EIT instrument.

EIT has a general cylindrical shape (figure (5)), mounted on the SOHO payload platform by means of 3 isostatic feet. It is used to avoid thermal stresses and keep a good alignment of the instrument.

The structure can be divided in two main sections: the telescope section with the optical components, the baffles and the mechanisms, and the camera part with the detector mounted at the end of a cold finger, itself connected to an external passively cooled radiator.

Several mechanisms have been integrated in the instrument:
- the rotating mask to select the bandpass,
- the shutter to define the time exposure,
- a filter wheel with various aluminium filters,
- a fixed additional aluminium filter,
- an electromechanical valve,
- an hermetic door, with a locking system redundant opening mechanism

As it is a single point failure, special care has been taken for the design and verification of the door system. A launch lock system is used to keep the door hermetically closed during the AIV and launch phase. It is released thanks to the linear extension of a paraffin actuator. The opening is performed with a stepping motor connected to a reduction gear system which produces the required torque. A redundant device ensures a good level of reliability, which in case of failure of the nominal system, opens definitely the lid with a spring system released by another paraffin actuator.

In order to save shutter activations, which may become a single point failure, half mask filters are available in the wheel mechanism to operate the camera in frame transfer mode. Half field of view (FOV) pictures are taken in this configuration.

2.3 Cleanliness.

The command electronics are common with the LASCO instrument, and integrated in the LASCO electronics box. This configuration is used to separate the optics and the electronics. On the camera, the detector is mounted in a vacuum tight compartment, with the pre-amplifiers outside the vacuum. This is to avoid contamination problems generated by electronic component outgassing under vacuum.

Due to the extreme sensitivity to contamination in the EUV wavelength regime, a major effort has been devoted to keep the instrument "clean". A witness mirror, coated with one stack of the multilayers was used to monitor the contamination status in the instrument during the AIV. The diagnostic is obtained after EUV reflectivity measurement of the witness sample, which reflects the status of the flight optics. Periodic checks ensured a good cleanliness level.

Moreover, the internal volume of the experiment is kept under low pressure (< 10 mbar) of dry nitrogen. This provides a good protection against contamination, but also against acoustic noise during AIV and launch, that may damage the extremely thin aluminium filters (2000 Å thick). This is obtained thanks to an hermetic entrance door and a good sealing of the external structural components. Periodic pumping during all the AIV phases has been performed. A specific umbilical connection through the launcher fairing will be installed to monitor the pressure and eventually pump the instrument to ensure an adequate low pressure for the launch.

The cooling radiator of the camera is also used to provide a cold finger at the back of the CCD. It is designed to trap the in-flight outgassed contaminants. Moreover, a heater is present on the cold finger, for periodic decontamination of the detector.

The entrance door will be periodically closed to isolate the instrument from the contaminant clouds produced by the thrusters during re-alignment procedures.

2.4 Stray-light.

Great attention was taken for the baffling of EIT. The rejection of the visible light at the level of the detector shall be efficient to a factor 10^{12}.

All the internal parts are black coated (black anodising of the aluminium). Each mirror of the telescope has its own baffle to stop the direct (EUV) light on the detector. A cross mask is applied in front of the primary mirror; its purpose is to suppress the cross talk between the 4 bandpasses. A front baffle is mounted and centred on the front part of the instrument. It has been designed to avoid stray-light and reflected light to other experiments when the door is open.

At the level of the entrance of the instrument, a set of wide aluminium filters is mounted in order to block solar visible and IR light, and to settle a well controlled internal thermal environment. To provide a better mechanical strength, they are made with a 60 nm plastic film and a wide supporting Ni grid (5 x 5 mm grid, 100 µm wide) encased between two 150 nm thick aluminium foils. They ensure a rejection of the visible better than 10^5. Moreover, the carbon contained in the plastic is used to reject light at wavelengths longer than 500 Å. A transmission close to 40 % is achieved in the band passes of the instrument.

Aluminium and aluminium/plastic filters can also be selected in a rotating wheel mechanism. They provide rejection factors up to 10^6.

Finally, an additional stray-light baffle has been introduced directly in front of the detector. It is also used to support a fixed pure aluminium filter.

Specific labyrinths are mounted at the periphery of the entrance filters, which occupy the main entrance section of the telescope, in order to provide a way for the remaining gas to flow around the filters. They are designed to block the visible stray-light with the same factor as the filters. The flow conductance of these labyrinths is higher than the valve used for pumping during AIV and for pressure equalisation before the first door opening in orbit. This will avoid any potential damage on the thin aluminium foils.

The filters are coated with interferential multilayers, with narrow bandpasses centred on the wavelengths of interest. The Zerodur substrate of the mirrors is coated with a layer of Boron, which defines the accurate aspherical shape. Successive coatings of Mo and Si layers with well defined thicknesses are applied. These parameters were computed and tested in order to provide a reflective constructive interference for a given wavelength. Second order peaks are suppressed by the aluminium filters. The 304 Å solar emitting line is very intense compared to the 284 Å one. Thus, the 284 multilayer stack has been specifically developed in order to have an efficient rejection factor for the 304 Å line. A ratio of 30 for the reflectivities between the 304 and 284 Å wavelengths has been achieved, after optimisation of all the successive thicknesses of the 30 layers.
To avoid cross talk between the four quadrants, a cross mask is applied in front of the primary mirror. The 284 and 304 Å quadrants are diagonally located for the same purpose.

2.5 Development philosophy.

The development of the instrument has been based on several models:

- one optical mock-up to verify the optical concept and image quality and another to settle and verify the alignment procedure,
- a structural model to verify the subsystem interfaces and to qualify mechanically the structure,
- qualification models of all the mechanisms,
- a protoflight model which underwent vibrations, EMC, TB/TV and calibration tests, as shown in figure (6),
- a set of spare flight mechanisms

In a protoflight scheme, the flight instrument must undergo all the tests at qualification levels, with acceptance durations. A complete set of tests is applied to the instrument.

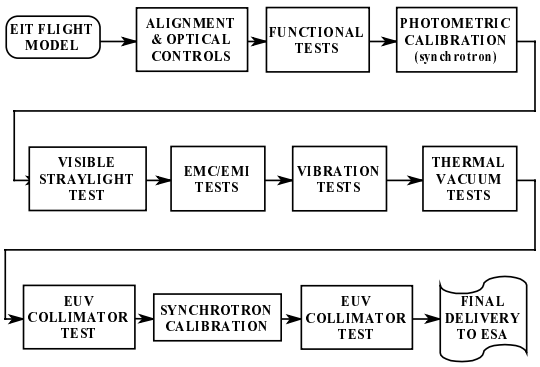

Figure (6): The development of the flight unit.

3. Alignment.

3.1 Alignment criteria.

The 4 telescopes combined in one require a non-classical method[1] to achieve an interferometric alignment of the optics. The mask on the primary mirror and the different thicknesses of the 4 coatings do not allow the use of a standard interferometer technique making use of Zernike polynomials.
The angle of view of main scientifical interest is 16 arcmin, it corresponds to the edge of the solar photosphere. Thus the alignment has been optimised for this angle which also corresponds to the best compromise when the misalignment effects and the FOV dependence of the aberrations are taken into account. The criteria are defined in table (1).

Spatial resolution: (circle of 80 % energy)	*2.6" for all FOV*
Wave front error: (at λ=633 nm)	*λ/15 at 16'*

Table (1): Alignment criteria.

3.2 Mechanical adjustment of the optics.

Great attention was taken to the fixations of the primary mirror and to the spacing between the telescope mirrors to maintain the optical quality. The distance between the primary and secondary mirrors has to be stable at 7 µm.
To avoid bending stresses in the mirror blank, the fixing is made by flexible blades and spherical bearings mounted on small Invar rods directly glued on the blank of the mirror before polishing. The primary mirror is first attached and aligned using a mechanical reference on the tube. Its back face will be use further as an optical reference.
The telescope final alignment will be achieved in the mounting of the secondary mirror. Five degrees of freedom will remain to be determined during the fine optical alignment. Some angular alignment between the two mirrors is also required to avoid cross talk. The final fixing is done with specific shims inserted between the secondary mirror support and its holding tube.

3.3 Alignment.

The use of interferometric methods in the visible has been preferred. A phase shifting interferometer and its associated software have finally been used to align the flight optics.
A specific procedure has been set up to achieve the wave front error measurement in each of the quadrants, and at various fields of view. The set up schematics is showed in figure (7). A dummy camera with a pin hole at the location of the CCD has been used, combined with an autocollimation flat mirror installed in front of the telescope aperture.
First, the interferometer spherical beam is focused on the pin hole of the dummy camera. A defocus of 150 µm corresponding to an optimisation at a 16 arcmin FOV is applied. Than, the secondary mirror position and orientation are adjusted in order to reduce and balance the WFE between the 4 quadrants.

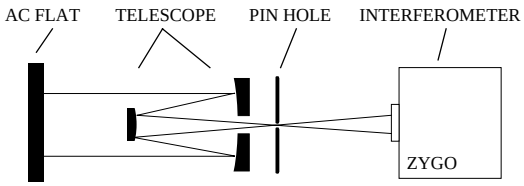

Figure (7): The alignment set up.

The specificity of this alignment comes from the division of the telescope in four quadrants with coatings of different thicknesses; this prevents to make use of Zernike polynomials to interpret the interferograms and to define the required corrections of the secondary mirror mounting.
Thus, analysis was performed on each quadrant taken separately. The results of the measurements are detailed in table 2.

FOV	Results (worst quadrant)
0 arcmin	*WFE < λ/14*
11 arcmin 30 arcsec (above)	*WFE < λ/11*
16 arcmin (left, right)	*WFE < λ/10*

Table (2): WFE measurements

With the WFE maps, it has been possible to compute the point spread function (PSF) at the operating nominal wavelengths, on each quadrant. A criterion to evaluate the image quality is the maximum diameter in which 80 % of the encircled energy lies. The results are in table (3).

FOV	171 Å	195 Å	284 Å	304 Å
0 arcmin	*1.9 ″*	*1.5 ″*	*1.4 ″*	*1.5 ″*
16 arcmin	*2.2 ″*	*1.7 ″*	*1.6 ″*	*1.9 ″*

Table (3): Size of the spot with 80 % encircled energy, in each quadrant, at their respective wavelength.

Thus the resolution is dominated by the pixel size[1,2] (2.6 x 2.6 arcsec).

3.4 Alignment of the camera.

The camera needs to be accurately mounted in order to locate exactly (± 50 µm) the CCD in the focal plane of the telescope. For this purpose, a dedicated spacer was design after trimming its thickness, and mounted between the camera and the telescope. This shim was defined after metrological measurements of the flight camera and the dummy camera used to align the optics. One shim per camera (flight and flight spare) was designed and manufactured.

4. Thermal status.

4.1 Design.

The thermal issue is a main concern for the sensor. The two main challenges are:
- the thermal control of the optical structure,
- the cooling of the detector down to -80°C.

Special care was taken to ensure the correct spacing between the telescope mirrors to maintain the optical quality. The two mirrors are mounted on each end of an aluminium cylinder, itself held to the main structure by a unique central flange to avoid thermal stresses.
The on-ground optical alignment is optimised for a 20°C environmental temperature. Once in orbit, due to the remaining inaccuracies of the thermal design, ageing effects on the thermal properties and sun flux variations, the equilibrium internal temperature will not be 20°C during all the observation periods.
Thus, the optical cylinder has been wrapped with thermofoil heaters and a set of thermistors. The thermal design has been computed and tested to reach a temperature lower than 20°C in all the in-orbit situations. The installed operational power on the optical cylinder shall be sufficient to increase the temperature to 20°C with the 8 Watts max allocated resources. Thus, the distance between the primary and the secondary mirror is made constant by means of this active thermal control. This configuration is the result of a trade-off study with the use of an Invar internal tube which has two drawbacks: more important mass and possible expansion due to ageing effects independent on temperature changes.

The CCD detector requires a very low operational temperature, around -80°C. This is to reduce the dark current to an acceptable value and mainly to increase the CTE by reducing the influence of the lattice defects induced by radiations. To achieve this requirement, the CCD is conductively connected to an external radiator with an important view factor with space. The selection of the radiator coating has been done to provide the highest heat rejection, it is a specific yellow paint with a high emissivity. To improve the efficiency of the cooling, an additional shield is mounted close to the radiator, directly on the platform of the S/C, to hide the hottest spacecraft parts still in the field of view.

4.2 Tests and verifications.

The thermal behaviour of the instrument has been extensively tested. All the components were thermal vacuum (TV) tested.
The temperature of the entrance aluminium filters facing the sun required all our attention. A first test in front of a sun simulator showed a quite high temperature environment around the filters. Thus, specific thermal tests were conducted. The filters are so thin that it is not possible to monitor the temperature of the aluminium foils with thermal sensors. Thermocouples were only used on the supporting frame. Measurements with a thermographic camera on a black spot deposited on the thin foil gave more accurate results in the centre of the filters. They were used to define the real thermal qualification range needed for these items.
After integration on the flight sensor, an instrument TV test was conducted. It proofed the good

functioning of the experiment under the qualification temperature range, and the ability to withstand extreme temperatures that are expected during spacecraft AIV, launch and in-orbit phases.
Then, a thermal balance (TB) test has been performed at instrument level. This test allowed a first correlation of the thermal mathematical model. It was also used to compute the size of a lateral radiating black area foreseen to reach a zero power temperature lower than 20°C.
At S/C level, a combined TB/TV test has been performed, in front of the large sun simulator in SIMLES, at ITS. The internal housekeeping thermistors were used in addition to the external thermocouples to monitor the thermal status of the EIT instrument under nearly flight conditions. This test revealed that the sun flux input on the external surfaces was underestimated. Flux estimation was only realistic with the real flight hardware (MLI on the flight harness) in front of a sun. The test correlation has been used to update the final thermal mathematical model. The main update concerned the MLI equivalent conductance, that was overestimated at unit level, because the external sun flux was not present during the instrument TB test (sun replaced by an equivalent sink temperature applied to a panel in front of the experiment) and were based on estimations.

5. Mechanical status.

5.1 Instrument studies and verifications.

A detailed mechanical analysis of the instrument has been performed during the B phase. The stress analysis under flight loads and vibration qualification tests showed appropriate safety margins. But the dynamical behaviour has been a major concern during the development and the AIV phases.
Among all the SOHO EID-A requirements, the most severe constraints for the EIT instrument are dictated by the vibration qualification specifications.
During the B phase of the project, acoustic vibrations were estimated by an equivalent random vibration test with a shaker. The initial PSD spectrum specification produced an equivalent rms acceleration of 11 g's at the basis of the sensor. During the project, this specification evolved to reflect the more accurate definition of the hardware and the test measurements on the SOHO structural model. The acoustic test on the complete flight spacecraft revealed quite low levels (1.9 g rms, "MEAS"), still far from the last updated specification (4 g rms, "EID-A 3") as detailed in figure (8).

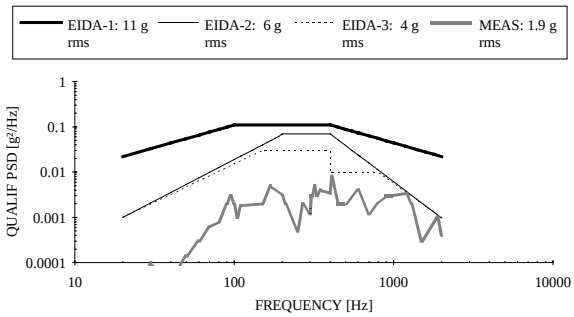

Figure (8): Evolution of the out of plane random vibration specification.

The development philosophy required an early qualification of the structure. It was based on the first vibration specifications. To follow the evolution of the specifications, the analyses were performed by using intensively the concept of effective masses. The dynamical analysis has been studied once by the main industrial contractor Spacebel Instrumentation, who established a finite element model of the instrument corresponding to the as-designed status at the beginning of the C/D phase. All the useful results of the dynamical studies can be summarised in the table 3.

Mode	f (Hz)	Meff X (kg)	Meff Y (kg)	Meff Z (kg)
1	137		8.795	
2	162	0.408		11.177
4	193	2.140	0.194	1.650
6	368	6.078	0.645	
7	373	1.234	1.932	
10	461	1.597		0.176

Table (3): Eigenfrequencies and associated effective masses of the complete instrument (static mass: 15 kg).

With these data and the modal damping factors ζ_i (estimated or measured), the dynamic mass[3] of the experiment mounted on the S/C can be computed according to equation (5.1):

$$M_{dyn}(\omega) = M_{st} - \sum_i \frac{M_{eff\,i} \cdot \omega^2}{\omega^2 - \omega_i^2 - 2i\omega\omega_i\zeta_i} \qquad (5.1)$$

where M_{effi} is the effective mass associated to the i^{th} eigenmode, $\omega = 2\pi f$, f is the frequency, $\omega_i = 2\pi f_i$, and f_i.is the i^{th} eigenfrequency.

This function of the frequency can provide the acceleration at the centre of mass of each vibration mode, knowing the acceleration of the basis. It gives also informations about the forces transmitted through the mounting interface on the S/C.

The response of the center of mass (COM) to the random vibration input can be computed[4] as per equation (5.2):

$$PSD_{com}(\omega) = \left| \frac{M_{dyn}(\omega)}{M_{st}} \right|^2 . PSD_b(\omega) \qquad (5.2)$$

where $PSD_b(\omega)$ and $PSD_{com}(\omega)$ are the input PSD at the bottom of the mounting feet of the experiment and the COM PSD.
All the mechanisms are mounted on the main cylinder. Thus, the PSD values at the COM are important for the experiment, as they can be used in a first approximation as the PSD levels for all these subsystems.

For example, the application of equation (5.2) truncated after 3 modes with the acceptance random levels specification along the optical axis for $PSD_b(\omega)$ gives the PSD at the COM. The latter is compared in figure (9) with the measurements of an accelerometer attached to the main cylinder.

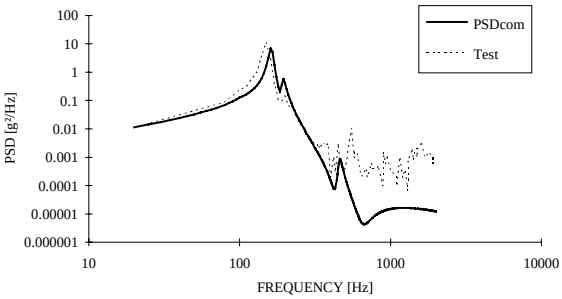

Figure (9): Comparison of the measured PSD (test) with the estimated COM PSD from equation (2).

The overall qualification cycle can be summarised in figure (10), where the SM structure, the qualification models of the subsystems and the flight model are tested separately, according to regularly updated levels. For example, EIDA-1 refers to legend in figure (8) in the case of the out-of-plane random test specification.

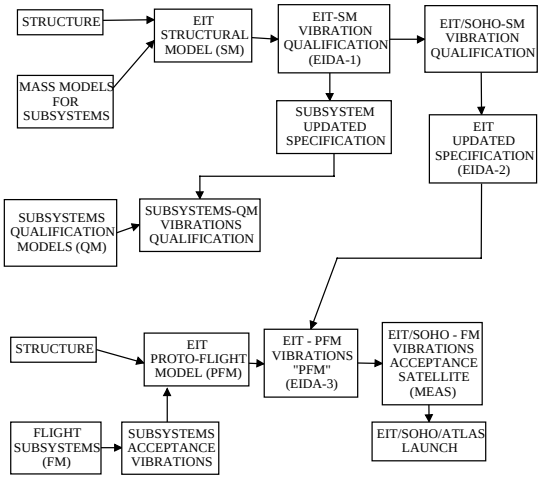

Figure (10): Mechanical development of EIT.

5.2 Pointing stability.

SOHO platform carries several science payloads and attitude determination sensors that require high pointing stability. To ensure this very severe pointing stability, thermoelastic calculations as well as microvibration (jitter) calculations were performed. These last calculations simulate the disturbances induced by the various payload mechanisms (mainly SUMER and UVCS), the tape recorders as well as the attitude control devices such as the four reaction wheels mounted on the platform. These computations were used to analyse and predict the line of sight jitter levels thereby induced. Calculations were correlated to tests on the S/C, in suspended and horizontal configurations; microvibrations were measured at the level of several experiments including EIT, the short term stability requirement of which is very severe: 1 arcsec stability over 15 minutes. Since EIT has no moveable legs which would allow to realign with the Fine Pointing Sun Sensor (FPSS), this FPSS has been placed close to EIT on the same platform.

6. Calibration.

To evaluate the real contribution of individual solar emission lines, with their associated temperature, it is mandatory to define exactly the 4 bandpasses of the instrument. For this purpose, all the spectral elements have been carefully calibrated[2], at subsystem and system levels.
The transmission of the aluminium filters was measured with the EUV light of the IAS synchrotron calibration facility (Orsay - Fr).

The reflectivity of the multilayers deposited on the mirrors was also characterised in the EUV wavelength range. The coatings on the primary and on the secondary mirrors are very similar.
The calibration of the detector in the EUV is of major interest for the instrument. Several series of tests were conducted to evaluate the relative sensitivity of each pixel and the average photometric properties of the CCD camera. These measurements were satisfactory, they showed a quantum efficiency higher than 25 % in all the bandpasses of EIT, which demonstrates that the EUV enhancement of the CCD was effective.

At system level, the overall sensitivity was measured on the flight model with the synchrotron beam and with an EUV collimator using classical line emission sources at 171 Å and 304 Å. Figure (11) shows an picture taken with the flight instrument in front of the EUV collimator. It is the image of a 70 lines/inch grid object illuminated at 171 Å with a Manson X-ray source.

Figure (11): Image at 171 Å.

Finally, this complex set of successive measurements provided enough informations to define the performance of the flight instrument. It is planned to gather additional useful informations by developing an additional model of EIT adapted for a sounding rocket payload. This program will make use of the available spare optical and mechanical components. Several sounding rocket launches are scheduled to update the in-flight performance of the SOHO instrument.

7. Lessons learnt

7.1 Alignment process.

During manufacturing process of theoretical components (polishing, aspherisation, coating, ...), the vertex and optical axis are known with a very good accuracy. This knowledge must be saved by the manufacturing of mechanical references aligned on these optical parameters (back face of the mirrors, outer diameter, holes for the mountings,...).

The design should be established to preserve access to these reference for the alignment.

The first steps of the alignment should make maximum use of these opto-mechanical references by means of classical (mechanical) metrological tools.

7.2 Mechanical development.

Overtesting should be avoided. Specifications and S/C measurements shall be carefully analysed and confronted to subsystems located in high amplification zones. Notchings are to be negotiated as soon as possible, to be further relaxed after updates of the S/C specifications.

We already noticed at the beginning of the project, by simple calculations, that the qualification tests leaded to higher levels at the COM of the experiment than the ones foreseen by the flight loads. This was a first indication that the qualification test levels were overestimated. These levels are generally taken as an envelope of all the possibilities with margins. Applying these levels, problems appear at the eigenfrequencies of the experiment. We warmly recommend to apply the procedure in place since a long time at JPL[5], which consists in measuring or at least limiting the transmitted force (by estimation knowing the dynamic mass of the instrument). The interface acceleration of the qualification tests are given as a simple function of the static mass which is obviously not correct. We could hope to be able to use in the future the Thevenin result[5]:

$$\frac{A}{A_0} + \frac{F}{F_0} = 1 \qquad (7.1)$$

where A and F are respectively the acceleration and the force (with their phase i.e. complex numbers) at the interface between the S/C and the instrument. A_0 and F_0 are respectively the acceleration and the force at the interface between the S/C and the experiment respectively when there is no experiment for A_0 (static mass of the experiment = 0) and when the interface if blocked for F_0 (static mass = ∞). Being given from ESA, A_0 and F_0 (which do not require any information about the

experiment), the experimenter after having computed the dynamic mass of his experiment, could evaluate the acceleration seen by his instrument at the interface with the S/C, as per equation (7.2).

$$A = \frac{A_0}{1 + \frac{M_{dyn,exp} . A_0}{F_0}} \qquad (7.2)$$

The relation (7.2) is difficult to be use in reality, but it has at least the benefit to show that the acceleration at the interface with the experiment is reduced at the eigenfrequencies of the experiment (where $M_{dyn,exp}$ is maximum) and that a notching should easily be accepted at eigenfrequencies with high effective mass for the given directions of excitation (which produces an important $M_{dyn,exp}$). The force at the interface is then defined by equation (7.3).

$$F = \frac{M_{dyn,exp} . A_0}{1 + \frac{M_{dyn,exp} . A_0}{F_0}} = \frac{F_0}{1 + \frac{F_0}{M_{dyn,exp} . A_0}} \qquad (7.3)$$

The final tests on the S/C showed that indeed levels were overestimated at the beginning of the program.

Concerning the acoustic tests, normally these tests are limited to the S/C. They are usually not needed at instrument level. We must be careful with this way of proceeding. During S/C acoustic test, the vibrations at the level of the CCD which is directly connected to the external radiator were measured very high. This could have been a direct effect of the acoustic wave on the radiator without passing through the platform and we had to verify by additional tests that the camera was correctly qualified by the only sine and random vibration tests at instrument and subsystem levels.

With the high acceleration levels (120 g) seen at the primary mirror location with the first EID-A specification, the preloading was not sufficient. Shocks occured when the ball bearings were in the clearance. With an unchanged EID-A specification, we would have to increase the preload if the mirror deformation remains acceptable, or we would have to change the support without clearance in the joints.

7.3 Thermal development.

Simles vacuum chamber appeared not to be adapted to such a large S/C and the test was not representative of the flight conditions. This was mainly due to multi-reflections between S/C parts and the Simles enclosure and non homogeneous sun flux. Moreover, some faces of the S/C were viewing non cooled parts of the vacuum chamber.

The use of a shroud with sink temperature to simulate the sun should be avoided when the surface of the experiment facing the sun has several coatings with different emissivities or when this face contains a cavity acting like a photon trap.

It is mandatory to evaluate at the earliest stage of the project the real behaviour of the thermal critical areas such as contact conductances, MLI efficiency, multiple reflections in photon traps appearing in baffles for example... This will avoid late additional thermal tests. Specific tests should be foreseen in the schedule to experimentally evaluate these parameters.

7.4 Calibration.

A realistic time slot should be preserved in the schedule at the end of the program to perform a complete calibration of the flight unit.

8. References.

[1] P. Rochus, "Alignment of the Extreme-UV Telescope (EIT)", in Applied Optics & Electronics Conference, IOP 5-8 Sep 94, York.

[2] JM. Defise et al, "Calibration of the EIT instrument for the SOHO mission", 1995, SPIE Proceedings 2517.

[3] A. Girard, J.F. Imbert, "Modal Effective Parameters and Trucation Effects in Structural Dynamics", 5th IMACS, pp 82-826,(1987).

[4] JM. Defise, "Dynamique d'une expérience spatiale: analyses et vérifications", in 3ème Congrès National Belge de Mécanique Théorique et Appliquée, Université de Liège, 30-31 May 94.

[5] T.D. Scharton, "Vibration-test force limits derived from frequency-shift method", Journal of Spacecraft and Rockets, vol 32, no 2, March-April 95, pp 312-316.